World Electric Vehicle Journal

MDPI

Article

An Anti-Skid Control System Based on the Energy Method for Decentralized Electric Vehicles

Longtao Ci, Yan Zhou and Dejun Yin *

School of Mechanical Engineering, Nanjing University of Science and Technology, Nanjing 210094, China
* Correspondence: yin@njust.edu.cn

Abstract: Anti-slip control, as a fundamental technique of vehicle stability control, prevents loss of control of vehicles, especially under extreme driving conditions. However, current control methods fail to suppress vehicle slippage when steering. Therefore, a new anti-slip control approach for four-wheel independent-drive electric vehicles (EVs) based on the energy method is proposed. This approach makes full use of the distribution of motor energy between the body and the wheels during vehicle turning, being able to adjust the driving torque of each wheel. Simulation results validate that the proposed approach can prevent wheel slip when the vehicle steers on slippery roads. Furthermore, simulations also show that the proposed control strategy can maintain high control performance when the motor flux linkage varies.

Keywords: anti-slip control; energy method; electric vehicle; motor flux linkage

1. Introduction

Driven by the energy crisis and environmental concerns, electric vehicles (EVs) have become a fast-growing product in recent years [1]. With the improvements in electric motor and motor controller technology, a wide range of powertrain configurations have been proposed [2,3]. One of the configurations is the distributed drive EV. With independently equipped motors for each wheel, it has many advantages, such as precise and measurable torque, fast torque response and simple actuation. These merits provide a wide perspective for vehicle dynamic improvement [4–6].

Wheel slip control as the basis of vehicle dynamic control plays a major role in maintaining vehicle stability [7–9]. Wheel slip occurs when the output torque of the actuator exceeds the maximum friction between the tire surface and the road surface. However, a variety of factors related to the road surface and vehicle state can affect the friction force, making it difficult to measure directly [10,11]. To solve this problem in vehicle dynamics control, there are two basic methods available: indirectly, by utilizing wheel slip ratios, and directly, using models for the vehicle or wheel. The main tasks of the former method are to estimate and control the wheel slip ratio. Fan used vehicle speed and wheel speeds to calculate the wheel slip ratio, and then used a fuzzy inference algorithm to estimate the optimal slip ratio [12]. The wheel speeds were measured through hall or magnetic speed sensors; however, calculation of vehicle velocity is difficult when all four wheels are being driven, and the vehicle absolute speed sensor is too expensive and not commonly available for application to actual vehicles [13]. In addition, due to current technical and cost limitations, it is impossible to determine the optimal slip ratio with precision [14]. Consequently, the aforementioned method is not appropriate for decentralized drive EVs. Some researchers focus on designing estimators that do not use direct vehicle speed. As an example, Fujii and Fujimoto proposed a novel estimator and observer to estimate slip ratios without the vehicle speed [15]. Xu et al. introduced a methodology for the on-line search of the optimal slip ratio under uncertain low grip conditions [16]. Despite their advantages, these methods are not always practical and robust. In addition, one should

check for updates

Citation: Ci, L.; Zhou, Y.; Yin, D. An Anti-Skid Control System Based on the Energy Method for Decentralized Electric Vehicles. *World Electr. Veh. J.* **2023**, *14*, 49. https://doi.org/10.3390/wevj14020049

Academic Editor: Joeri Van Mierlo

Received: 26 December 2022
Revised: 30 January 2023
Accepted: 8 February 2023
Published: 10 February 2023

bear in mind that the anti-skid capability in the tire-road interaction greatly depends on the pavement conditions, including in particular on the texture and skid resistance of the road's surface [17].

In contrast to indirect methods that rely on wheel slip ratio, direct methods based on a model of the vehicle or wheel not only do not depend on optimal slip ratio, but also do not require knowledge of the chassis speed. Sakai et al. developed a novel model following control (MFC) system which has been validated and further improved for preventing wheel slip [18,19]. This method unifies the non-slip wheels and the vehicle body into a nominal model, and regards wheel slip as the reduction of the overall equivalent moment of inertia. When the torque output by the actuator is applied to the nominal model and the actual vehicle, the actuator's torque output is adjusted simultaneously. To improve the performance of the MFC, Yin et al. proposed a novel data fusion method based on MFC to control wheel slip [20]. Nevertheless, the MFC-based driving anti-skid method is based on a rough vehicle model, preventing adaptation to the variation in vehicle mass, so an equivalent weight transfers due to vehicle longitudinal movement. Yin et al. proposed a novel traction control based on maximum transmissible torque estimation (MTTE) [21]. This approach does not adopt a whole-vehicle system, but rather focuses on a single wheel. Furthermore, it does not depend on the estimation of vehicle speed or slip ratio. Instead, it estimates the longitudinal friction force on the tire from the torque and speed of the electric motor driving it. MTTE is easy to implement and compatible with numerous tire-road conditions [22]. However, MTTE is based on a quarter-body model, which does not consider the fact that the four wheel speeds of a vehicle are different during cornering. Therefore, using a uniform vehicle speed for the whole vehicle control in a cornering situation will produce a poor control effect [23,24]. Besides, MTTE's effective operation is based on some basic assumptions, for example, the output torque being able to work accurately on the vehicle. However, when being driven, the temperature rises, and aging of the driving motor will lead to the decrease of the motor flux linkage [25]. These will affect the accuracy of the output torque, resulting in a decrease in the control method's performance.

The problems with the control methods mentioned above are mainly concentrated in two aspects:

1. In turning conditions that are prone to loss of control, the control methods fail to ensure stable driving of the vehicle;
2. The performance of these control methods is susceptible to variations in motor parameters, which cannot be avoided in real vehicles.

To solve the aforementioned problems, the additional motion of each wheel was studied when the vehicle was turning; and using the characteristics of the distributed drive motor and the wheel corresponding to each other, a novel anti-slip control approach is proposed based on energy method. This approach can not only be applied for straight line motion, but when turning; furthermore, it incorporates the motor power following method, enabling anti-slip control to eliminate precise motor torque, improving the stability and effectiveness of this anti-slip approach.

The rest of this paper is organized as follows: in Section 2, the novel anti-slip control strategy is developed; Section 3 presents the EV modelling; in Section 4, numerical simulations are described for different control cases; Section 5 covers experiments designed to validate the proposed control algorithm; and conclusions are drawn in Section 6.

2. Wheel Slip Control Approach

2.1. Control Strategy

When a distributed drive vehicle is moving on a flat surface without any slippage, the generated energy of the motor is ideally converted into kinetic energy for the movement of the vehicle, which includes the body kinetic energy and the wheel kinetic energy; the kinetic energy consists of translational kinetic energy and rotational kinetic energy. Therefore, on the simplifying assumption that the moment of inertia of the transmission system is

ignored, when the vehicle is driving in a straight line in a normal manner, the kinetic energy of the vehicle's body can be simplified as

$$E_b = \frac{1}{2} M_b u^2 \tag{1}$$

where M_b represents the body mass, and u is the longitudinal speed of the chassis.

Meanwhile, the kinetic energy of each wheel during the plane motion is presented as

$$E_i = \frac{1}{2} m u_i^2 + \frac{1}{2} J_\omega \omega_i^2. \tag{2}$$

Here, m is the mass of the wheel, u_i is the longitudinal speed of the ith wheel (i = 1, 2, 3, and 4), J_ω is the inertia of the wheel, and ω_i denotes the rotation angular velocity of the i^{th} wheel (i = 1, 2, 3, and 4). In Equation (2), $\frac{1}{2} m u_i^2$ represents the translational kinetic energy of the wheel, and $\frac{1}{2} J_\omega \omega_i^2$ denotes the rotational kinetic energy of each wheel.

From Equation (1), the calculation of energy requires the participation of speed, but the control strategy can achieve an acceptable control effect without precise speed estimation. Here, the median value of the speeds of the four wheels are used, which can be measured by wheel speed sensors, as the reference vehicle velocity. Accordingly, the relationship between wheel velocity and vehicle velocity is shown as follows:

$$\begin{cases} u_i = u, \\ \omega_i = \frac{u}{r}. \end{cases} \tag{3}$$

Combined with Equations (1)–(3), the total kinetic energy of the vehicle, which represents the energy of the motor output under normal conditions, can be expressed as

$$E = E_b + \sum E_i = \frac{1}{2} M_b u^2 + 2mu^2 + 2J_\omega \frac{u^2}{r^2}. \tag{4}$$

Hence, during the linear motion, the relationship between the wheel rotation kinetic energy E_{ω_i} and the vehicle kinetic energy E is:

$$k_i = \frac{E_{\omega i}}{E} = \frac{J_\omega}{(M_b + 4m) r^2 + 4J_w}. \tag{5}$$

This formula indicates that when the vehicle is driving straight without any slippage, the ratio k_i is a constant value, which can be used to control the vehicle from skidding.

Applying the above method and assumption for turning conditions, the body and wheel kinetic energy are expressed as follows:

$$E_b = \frac{1}{2} M_b \left(u^2 + v^2 \right) + \frac{1}{2} J \omega_r^2 \tag{6}$$

$$E_i = \frac{1}{2} m \left(u_i^2 + v_i^2 \right) + \frac{1}{2} J_\omega \omega_i^2 \tag{7}$$

where v is the lateral velocity of the vehicle, J is the body moment of inertia, ω_r is the yaw rate of the vehicle, v_i stands for the lateral speed of the ith wheel, and J_ω represents the inertia of the wheel.

When the vehicle is turning, the Ackermann steering model is usually used to calculate the expected rotational speed of the four wheels of the vehicle. However, in actual steering, due to the influences of body yaw and lateral speed, the Ackermann steering model is only suitable for very low speeds, and the yaw and lateral speed of the vehicle exert little influence on the vehicle. Therefore, the reference speed of each wheel is estimated based on the rigid geometric structure of the vehicle and stacking the yaw rate.

Taking the front left wheel as an example, as shown in Figure 1, O is the center of mass (CM) for the vehicle; u, v and ω_r denote the longitudinal velocity, lateral velocity,

and yaw rate of the chassis, respectively, where u and v are estimated according to the method proposed above and ω_r is measured by the inertial sensor at the vehicle center of mass. u_i and v_i represent the longitudinal and lateral reference velocity at each wheel center, respectively; l_{OFL} is the horizontal distance from the vehicle centroid to the wheel center; b is half of the wheelbase; $v_{\omega r1}$ is the velocity of the yaw rate acting on the center of the left front wheel, where $v_{wr1} = \omega_r \cdot l_{OFL}$. As shown in Figure 1, the proposed steering kinematics is assumed under a left turn.

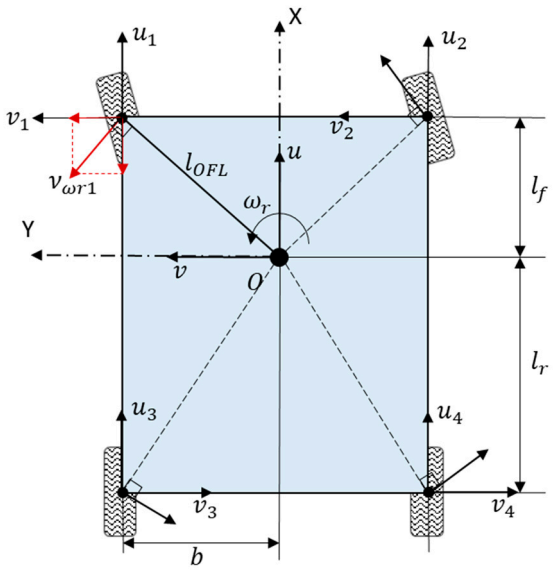

Figure 1. Vehicle model used for velocity estimation.

From the geometric relations, the reference velocity u_i and v_i of each wheel center can be calculated as:

$$\begin{bmatrix} u_1 \\ u_2 \\ u_3 \\ u_4 \end{bmatrix} = \begin{bmatrix} 1 & 0 & -b \\ 1 & 0 & b \\ 1 & 0 & -b \\ 1 & 0 & b \end{bmatrix} \begin{bmatrix} u \\ v \\ \omega_r \end{bmatrix}, \tag{8}$$

$$\begin{bmatrix} v_1 \\ v_2 \\ v_3 \\ v_4 \end{bmatrix} = \begin{bmatrix} 0 & 1 & l_f \\ 0 & 1 & l_f \\ 0 & 1 & -l_r \\ 0 & 1 & -l_r \end{bmatrix} \begin{bmatrix} u \\ v \\ \omega_r \end{bmatrix}. \tag{9}$$

Accordingly, the energy of the whole vehicle under two-dimensional motion is determined as

$$E = E_b + \sum E_i = (M_b + 4m)\left(u^2 + v^2\right) + J\omega_r^2 + 4m\left(l_f - l_r\right)\omega_r v + 2m\left(l_f^2 + l_r^2 + 2b^2\right)\omega_r^2 + J_\omega \sum \omega_i^2. \tag{10}$$

The ratio between the kinetic energy of wheel rotation and the kinetic energy of the whole vehicle is defined as

$$k_i' = \frac{E_{\omega i}}{E} = \frac{J_\omega \omega_i^2}{(M_b + 4m)(u^2 + v^2) + J\omega_r^2 + 4m\left(l_f - l_r\right)\omega_r v + 2m\left(l_f^2 + l_r^2 + 2b^2\right)\omega_r^2 + J_\omega \sum \omega_i^2}. \tag{11}$$

As can be seen from the above, in the ideal case, k_i' is close to a constant value just like k_i. When wheel slip occurs, the wheel speed increases abnormally. Simultaneously, the rotational energy of the wheel increases; the kinetic energy of wheel rotation increases abnormally as a percentage of the total motor output. Hence, k_i' is used to characterize wheel slippage as a characteristic variable, not only for straight-line conditions, but also for steering conditions.

2.2. Controller Design

Figure 2 illustrates the design of the controller, in which the vehicle anti-slip algorithm is expected to realize the control of motor command power according to the prevailing dynamic situation. When the vehicle drives stably without slipping, the reference power P_i^*, which is calculated by multiplying the reference torque T^* and the ideal wheel speed ω_i^*, is expected to pass without effect. On the other hand, When the vehicle skids, the controller can reduce command power input to the motor, thus constraining the motor output torque.

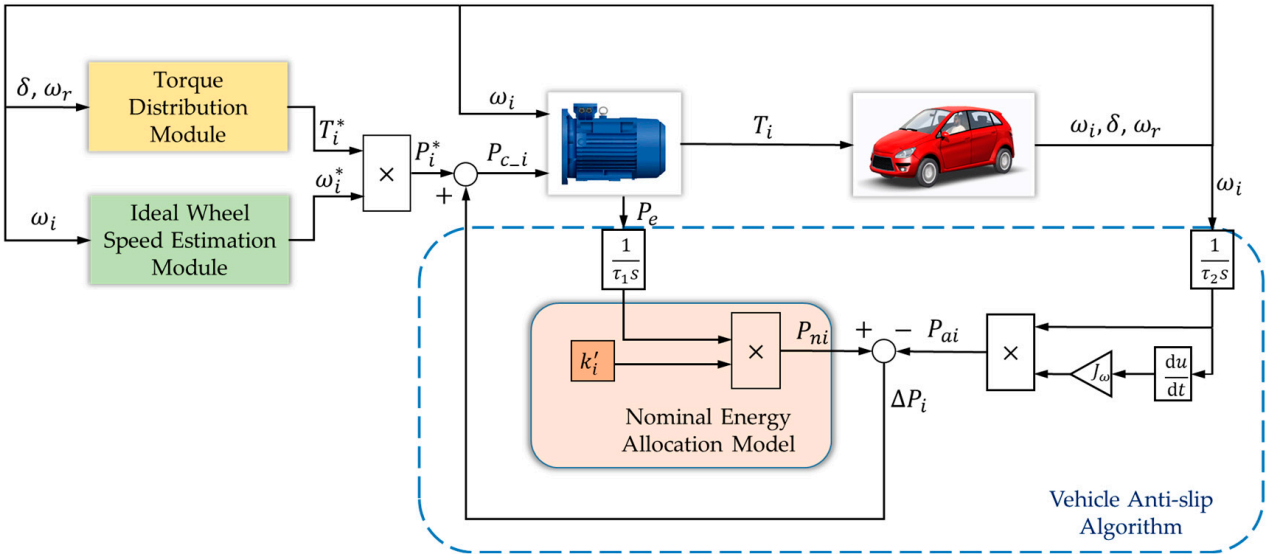

Figure 2. Control system based on energy method.

First, as shown in Equation (12), the nominal energy allocation model uses the motor actual output power P_e and characteristic variable k_i' to calculate nominal P_{ni} that should be consumed when the wheels are not skidding. Then, according to the rotational speed and the moment of inertia of each wheel in the actual motion state of the vehicle, the wheel rotational power consumed in the actual motion state can be obtained, as described in Equation (13). Here, T_i is the torque applied to the ith wheel, which can be obtained as $T_i = J_\omega \dot{\omega}_i$. Combining Equations (12) and (13), the adjustment power ΔP of each wheel are acquired in (14). Finally, the controller utilizes the adjustment power value to adjust the reference power P_i^* for obtaining the commanded power P_{c_i}, and the commanded power and actual wheel speed signals are used by the motor to generate drive or braking torque for the vehicle.

$$P_{ni} = P_e k_i' \tag{12}$$

$$P_{ai} = T_i \omega_i \tag{13}$$

$$\Delta P_i = P_{ni} - P_{ai} \tag{14}$$

Considering the variety of working conditions, and to make a fair comparison between the proposed algorithm and other algorithms, the control system adopts an average torque distribution method to distribute reference torque T^* [26]. The steering wheel angle δ and yaw rate ω_r signals required by the torque distribution method are obtained by commonly used sensors. In addition, the ideal wheel speed estimation module based on Equations (8) and (9) can estimate the wheel speeds, which ensures that no wheel slip occurs. For smoothing of the digital signals ω_i and P_e, a low-pass filter (LPF) is introduced in the control system; the time constant of τ_1 is set to 50 ms as for τ_2.

3. EV Modelling

This section describes the building of a dynamic EV model by using MATLAB™/Simulink coupled with CarSim, which is driven by four independently controlled PMSM motors. The chassis layout is shown in Figure 3. The controller receives power and rotation speed signals from four motors, and then sends the power command signals to them.

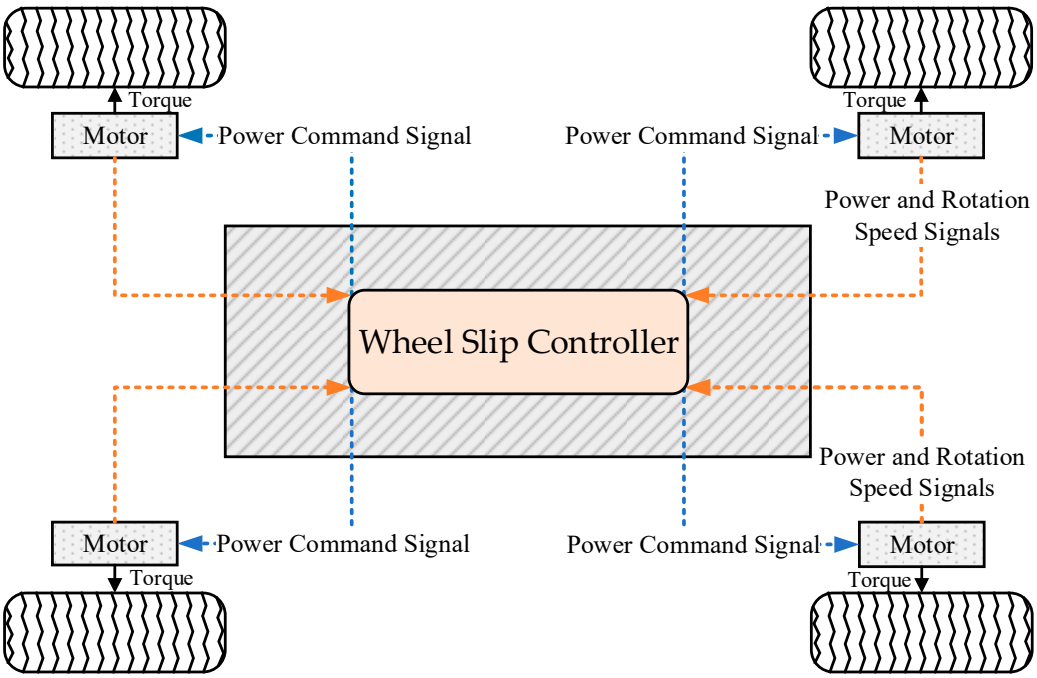

Figure 3. Chassis and wheel slip control system layout.

3.1. Vehicle Dynamic Model

To simulate vehicle response under various maneuvers, it is essential to develop a detailed and comprehensive vehicle model. Therefore, the commercial vehicle dynamics software, CarSim, was introduced to conduct this study. To simulate a real vehicle, CarSim uses an embedded vehicle model that contains the following components: a driver model, a brake and steering system, a Pacejka 5.2 tire model, and suspension components.

3.2. Motor Model

A permanent magnet synchronous motor was chosen as the power source of the EV model because of its high corresponding torque and high efficiency. To achieve motor power following control, the direct power control method (DPC) proposed in [25] was adopted. As shown in Figure 4, the control scheme includes the stator windings instantaneous power calculation, the power hysteresis, and the optimal switching table. This method has a simple form of control and enables the reactive power of the input motor to be controlled at 0, resulting in a power factor close to 1.

Given that the reactive power reference value is $q_s^* = 0$, the active power reference value is p_s^*, where p_s^* is the vehicle controller output command power P_c. The two reference values are passed through a DPC output inverter switching signal, thus realizing the closed-loop control of the motor, and simultaneously outputting the actual output power P_e and voltage switching status of the motor S_{abc}. Finally, the PMSM outputs torque T using sensor-measured current values i_{abc} and actual wheel rotation speed ω.

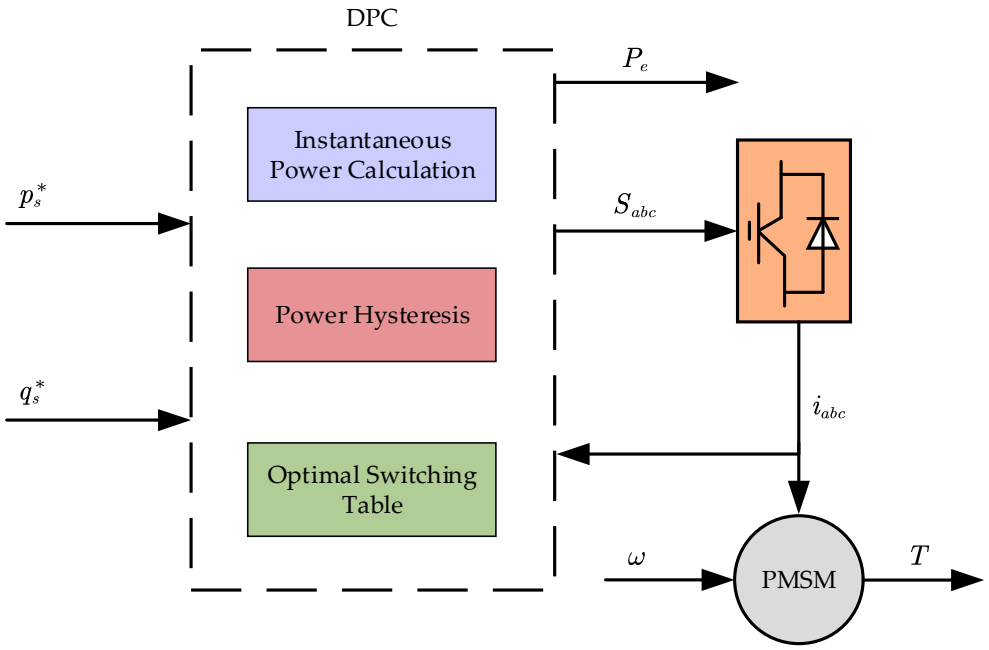

Figure 4. DPC control scheme for PMSM.

4. Simulation and Results

Various CarSim-Simulink simulations were used to verify the effectiveness of the proposed anti-slip control system. Table 1 summarizes the specifications of the test vehicle, which is a type of B-class passenger car. Table 2 lists the parameters of the motor, and Figure 5 presents the torque speed diagram of the motor. In addition, the power source and other transmission components are set as external inputs in the transmission system settings, and the gear ratio is set to 1. The torque is directly applied to the wheels to achieve the simulation of the decentralized vehicles.

Table 1. Vehicle parameters.

Parameter	Value
Vehicle mass M	1230 kg
Sprung mass M_b	1110 kg
Wheel mass m	30 kg
Half-wheelbase b	1.300 m
Front wheelbase l_f	1.040 m
Rear wheelbase l_r	1.560 m
Vehicle yaw inertia J	1343.1 kg·m^2
Wheel inertia J_ω	0.6 kg·m^2
Wheel radius r	0.31 m

To evaluate performance of the proposed control approach under an actual driving environment, a mechanism of white noise is added to each feedback state. The noise is added on to the measured data of each wheel according to the data from a real sensor: WA AU7428N200 (Tamagawa Seiki Co., Ltd., Nagano Prefecture, Japan). The noise for acceleration on the CM is up to 0.049 m/s^2. The noise for the yaw rate reaches 1 deg/s. The noise effect for the wheel speed occurs up to 15 rpm.

Additionally, the anti-slip control system based on the MTTE presented in [20] is used, as shown in Figure 6, for the following comparison. In the following simulations, the same vehicle parameters are adopted for comparison: τ_i is equal to τ_1, and α is set to 0.9.

Table 2. PMSM parameters.

Parameter	Value
Stator resistance R_s	0.958 Ω
Number of pole pairs p_n	8
D-axis inductance L_d	5.25 mH
Q-axis inductance L_q	5.25 mH
Permanent-magnet flux linkage ψ_f	0.287 Wb
DC-link voltage U_{dc}	560 V
Rated power P_N	45 kW
Rated current I_A	99 A
Rated torque T_{eN}	340 N · m
Maximum power P_m	110 kW
Peak current I_{peak}	280 A
Maximum torque T_m	850 N · m
Torque coefficient K_T	3.44 Nm/A
Back-electromotive force coefficient K_e	170 V/krpm

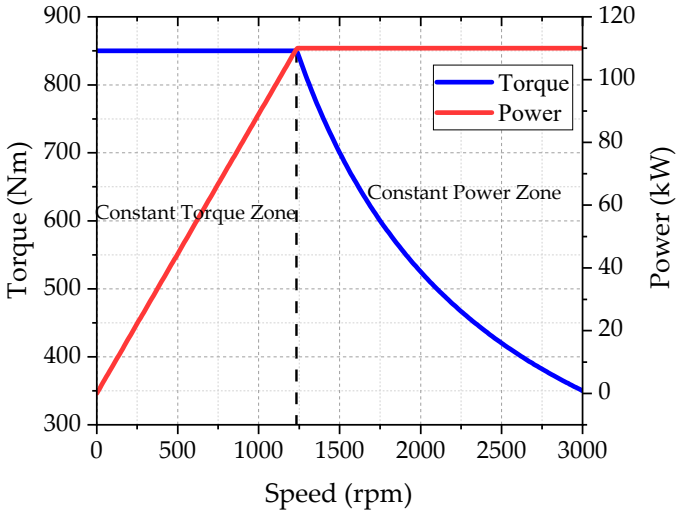

Figure 5. Torque speed diagram of the motor.

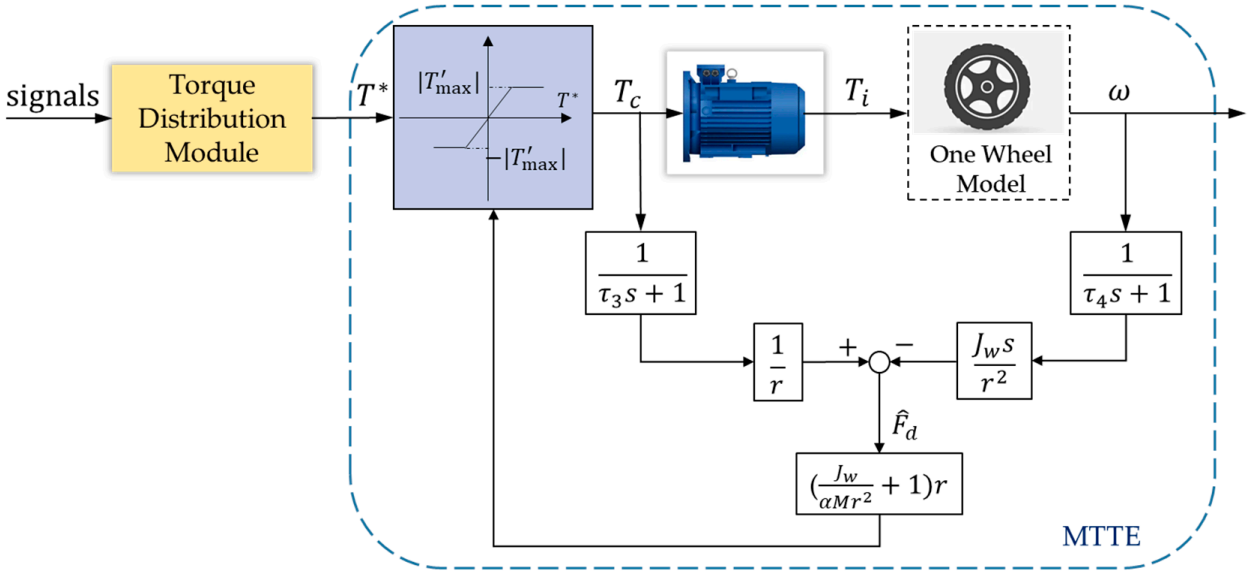

Figure 6. Control system based on MTTE.

4.1. Straight Line

Under straight line driving conditions, the vehicle drives on a jointed road. The jointed road has a coefficient of adhesion of 0.8 from 0 to 20 m, which changes to 0.2 for the next 20 m, and then to 0.8 until the end. The initial speed is set to 30 km/h and the torque command value for a single drive motor is set to 250 N·m.

It is noteworthy that the performance of all four wheels is approximately the same when driving in a straight line, so, herein, this research only shows the simulation results of the front left wheel. Figure 7a reveals the change of the wheel speed following the speed of the chassis. Figure 7b displays the variation in the slip rate of the front left wheel. Figure 7c presents the longitude force during driving. After the vehicle (without control) enters a stretch of low-adhesion road from one exhibiting high adhesion, the road adhesion condition decreases rapidly. At this time, the motor output torque is too large due to the non-application of anti-slip control. Consequently, the drive wheel accelerates rapidly and then appears to over-slip as shown in Figure 7a,b. At this point, the longitudinal traction of the wheel is not fully utilized, resulting in a significant decrease in the longitudinal force as illustrated in Figure 7c.

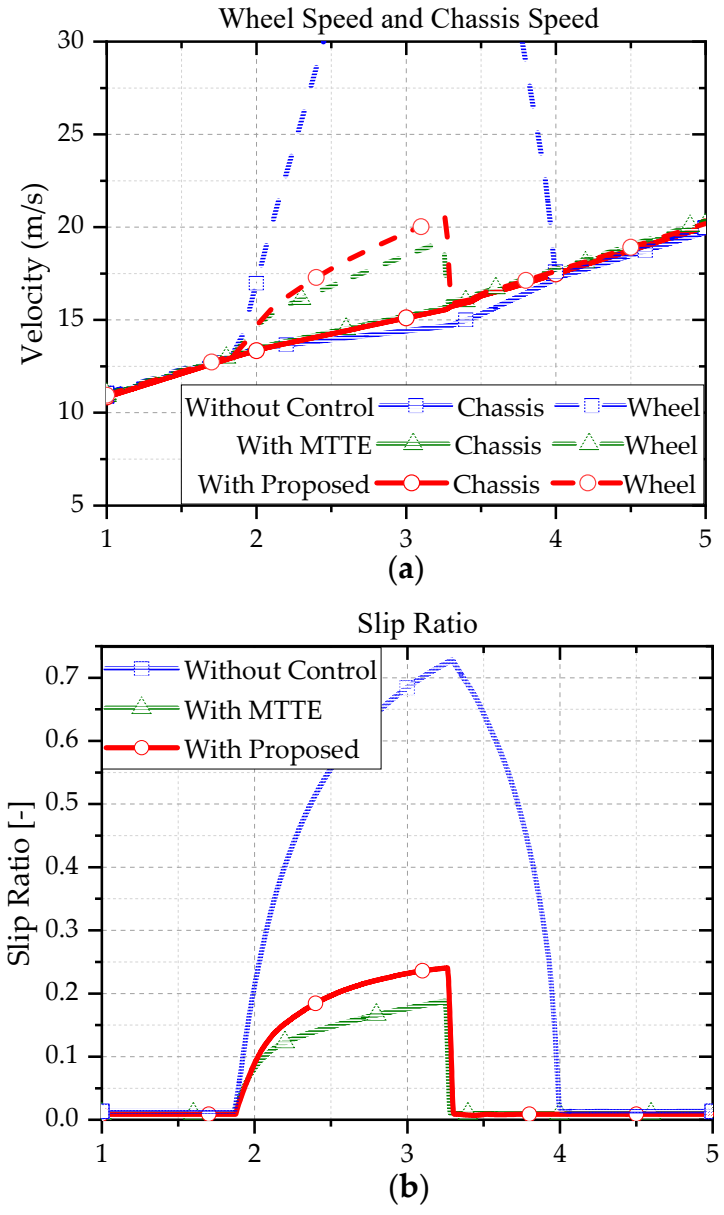

Figure 7. *Cont.*

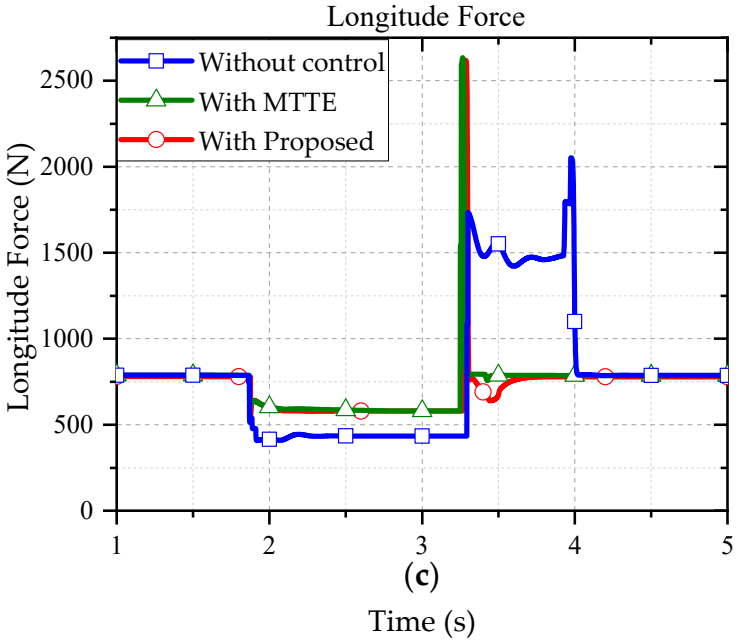

Figure 7. Comparison of the vehicle's front left wheel without control, with MTTE and with proposed approach: (**a**) wheel speed and chassis speed; (**b**) slip ratio; (**c**) longitudinal force.

However, MTTE and the control strategy proposed herein can quickly adjust the output torque and the power of the motor depending on the abnormal change of the wheel speed, so that the vehicle can make full use of the adhesion to continue moving on the low-adhesion road surface. According to the simulation results, after 5 s of straight-line acceleration on the jointed road, the final speed of the vehicle without control is 19.22 m/s. With anti-slip control strategy, the final speed of the vehicle is over 20 m/s: the anti-slip control not only ensures the driving safety of the vehicle, but also enables the tires to make full use of the road surface adhesion conditions and improve driving ability.

4.2. Sine with Dwell Simulation

To assess the superiority of the proposed approach compared with MTTE in steering conditions, sine with dwell control is tested to Federal Motor Vehicle Safety Standards (FMVSS) 126 requirements. In FMVSS 126 requirements, the vehicle response is evaluated using lateral displacement and the yaw rate: at 1.07 s, the lateral displacement of the vehicle mass center must be 1.83 m or greater relative to the start of the test; at 1 s after the steering stops, the instant yaw rate must be less than 35% of the peak yaw rate; at 1.75 s after the steering stops, the instant yaw rate must be less than 20% of the peak rate; otherwise, the vehicle fails the test [27].

In this study, according to the standards, the initial speed is set to 80 km/h and the friction coefficient is 0.7. The steering wheel angle is depicted in Figure 8a, and its amplitude is 300°. Moreover, Figure 8a describes the comparison of the yaw rate between the vehicle with the proposed approach and MTTE. Figure 8b presents the lateral displacement of the two methods. On a high-adhesion road, both control approaches can meet the requirements of lateral displacement and yaw rate. Furthermore, the convergence speed of the yaw rate of the proposed approach is faster than that of MTTE, and the yaw rate of the proposed approach is much closer to the target yaw rate, which preliminarily proves that the proposed algorithm is more flexible in turning scenarios.

To reflect the control effect between the two approaches more clearly, the road adhesion coefficient is set to 0.5 to simulate a slightly wet road. Figure 9 presents the yaw rate and lateral displacement on a low coefficient surface. Table 3 displays the evaluation results of the sine with dwell test. The results indicate that the vehicle with MTTE fails the test whereas the vehicle with the proposed control system passes.

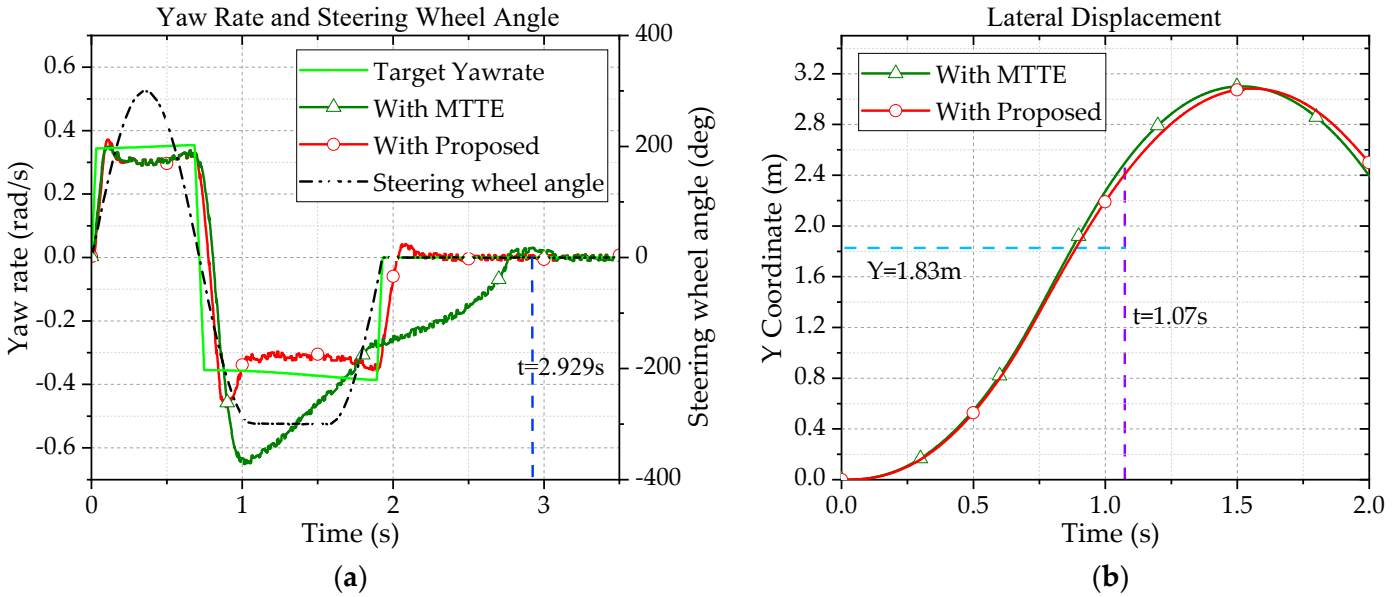

Figure 8. Sine with dwell simulation results on a high-adhesion road: (**a**) the yaw rate and steering wheel angle; (**b**) lateral displacement.

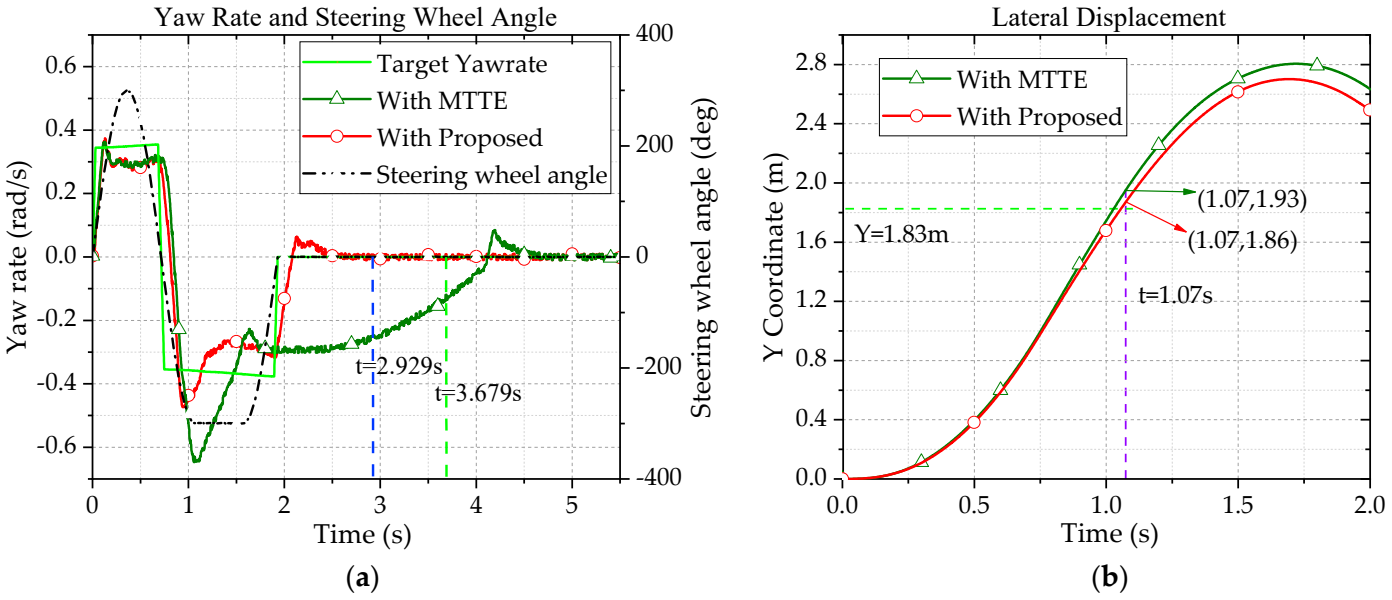

Figure 9. Sine with dwell simulation results on a low-adhesion road: (**a**) yaw rate and steering wheel angle; (**b**) lateral displacement.

Table 3. Evaluation of the sine with dwell test.

Yaw Rate	Proposed Control	MTTE
Peak value	−0.475 rad/s	−0.645 rad/s
35% of the peak value	−0.166 rad/s	−0.226 rad/s
1 s after completing steering	−0.003 rad/s	−0.256 rad/s
20% of the peak value	−0.095 rad/s	−0.129 rad/s
1.75 s after completing steering	−0.002 rad/s	−0.133 rad/s

Figure 10 shows the intermediate results between the vehicles with MTTE and proposed control, including wheel speed, wheel slip ratio, longitudinal tire force, lateral tire force, and yaw moment. When a four-wheel distributed vehicle turns, there will be a

speed difference between the left and right wheels. To prevent the wheels from slipping, as shown in Figure 10a,b, MTTE will limit the speed of each wheel to the speed of the vehicle according to Equation (15). Therefore, the speed difference between the left and right wheels is reduced, increasing the tendency to understeer. Moreover, excessively restricting the wheel speed will cause the slip ratio to be too low according to Figure 10c,d, which is far from the optimal slip ratio. In particular, at around 2 s, when the vehicle makes a leftward turn to move the vehicle back to right, the wheel slip rate is limited near the value of 0. According to the tire dynamics, the wheel longitudinal force is also limited to a low value, which contributes little to the yaw moment and cannot provide enough moment to move the vehicle back to the right. As a result, as presented in Figure 10g,h, the tire lateral force maintains a large value even after 2 s, which aggravates the understeer of the vehicle. Figure 10i,j further illustrate that the longitudinal force's yaw moment is very small, and combined with the lateral force's yaw moment, it is not enough to bring the vehicle back into alignment. Eventually, the vehicle with MTTE fails the test.

$$T_{\max} = T + \frac{J_\omega}{r}\left(\frac{1}{\alpha}\dot{V} - \dot{V}_\omega\right), \alpha = 0.9 \tag{15}$$

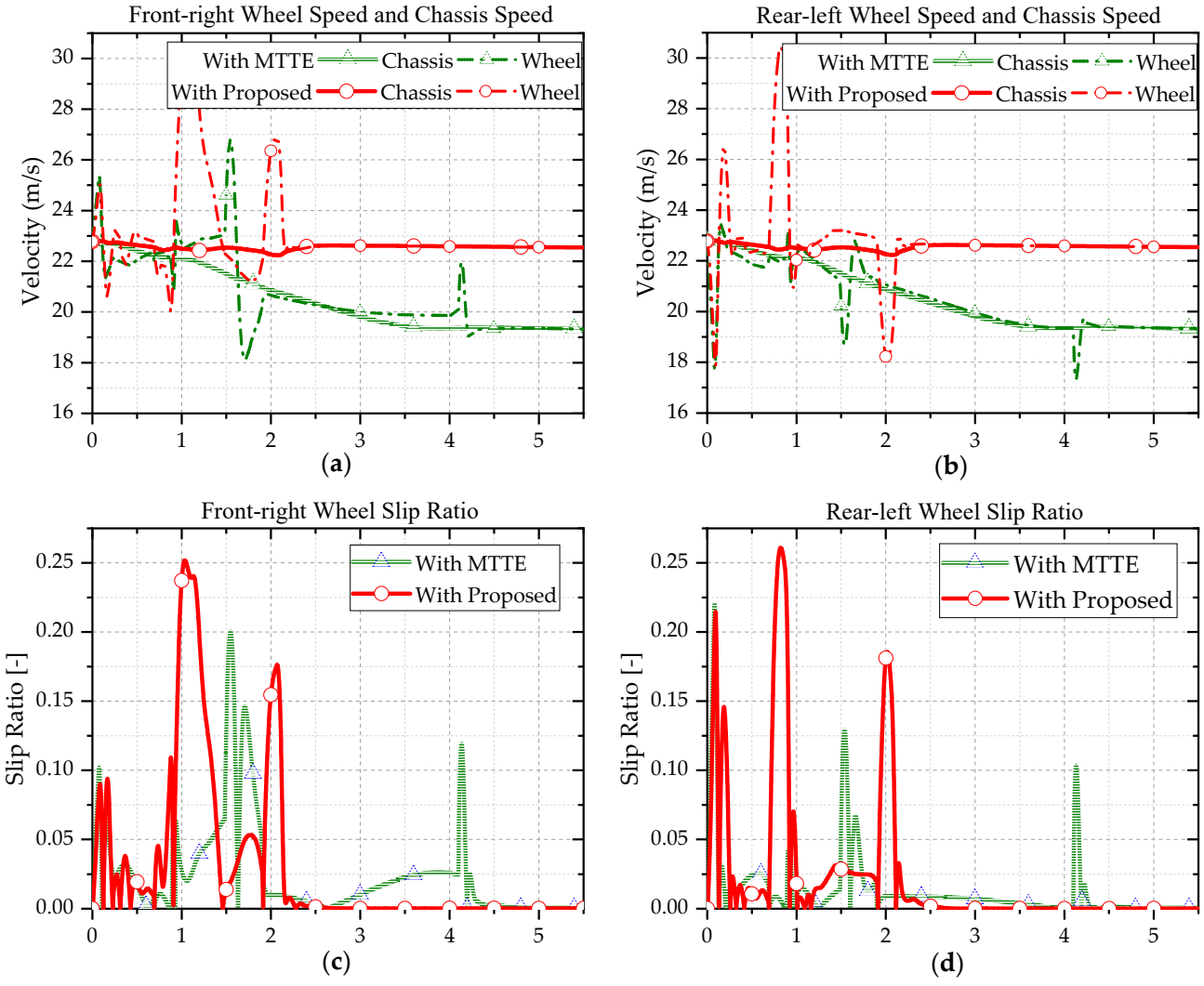

Figure 10. *Cont.*

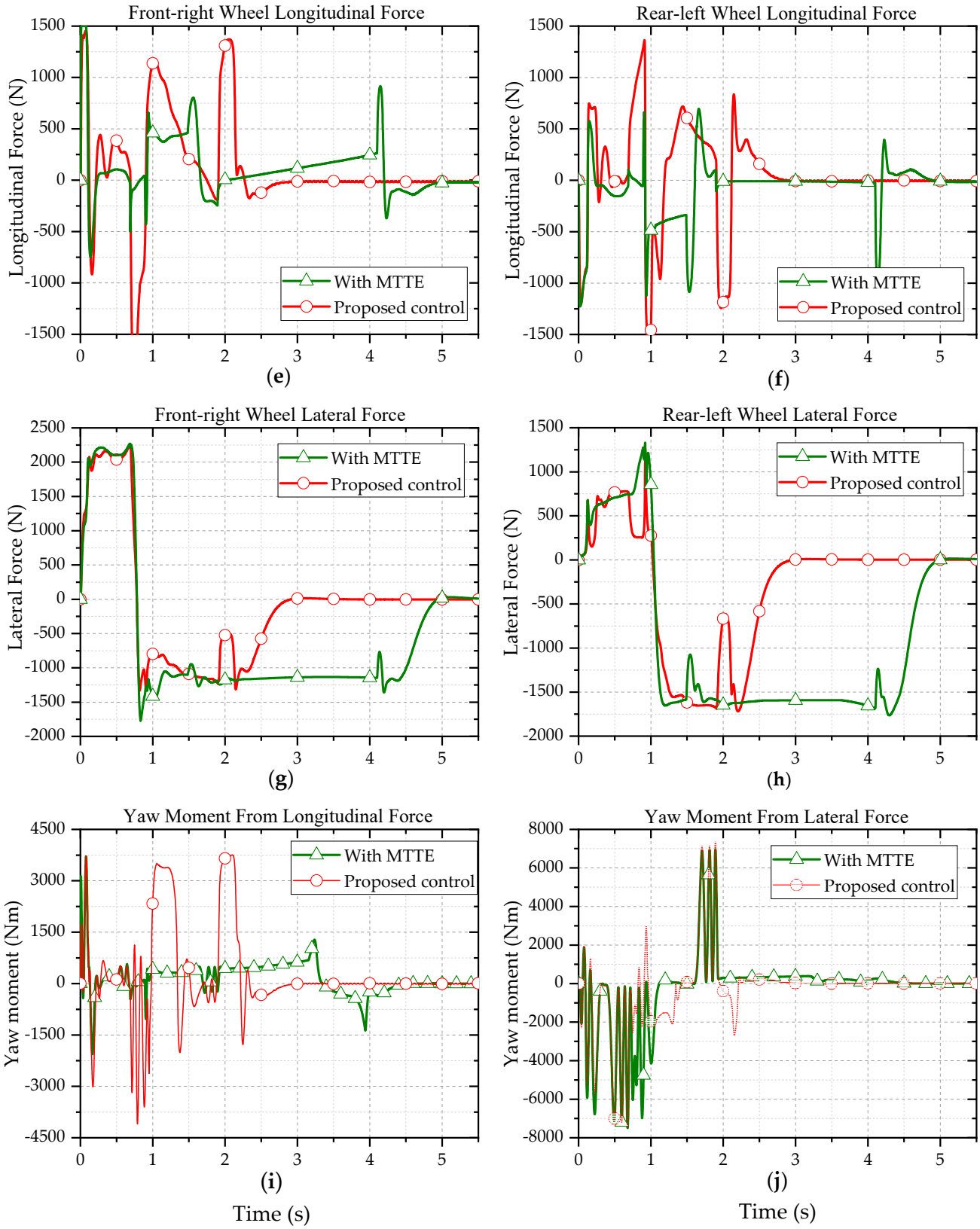

Figure 10. Comparison of intermediate results for sine with dwell: (**a**) front-right wheel speed and chassis speed; (**b**) rear-left wheel speed and chassis speed; (**c**) front-right wheel slip ratio; (**d**) rear-left wheel slip ratio; (**e**) front-right wheel longitudinal force; (**f**) rear-left wheel longitudinal force; (**g**) front-right wheel lateral force; (**h**) rear-left wheel lateral force; (**i**) yaw moment from longitudinal force; (**j**) yaw moment from lateral force.

By contrast, the proposed approach takes the optimal speeds of four wheels in two-dimensional motion into account, which not only prevents wheel slip, but also maintains the speed difference between the left and right wheels. As illustrated in Figure 10c,d, the front-right and rear-left wheel slip ratios are both near the optimal slip ratio when the vehicle steers left and right. Therefore, as displayed in Figure 10e,f,i, the right front and left rear wheels are able to make full use of the traction provided by the surface to the tires, to contribute yaw moment for turning by driving or braking. Furthermore, according to the tire force ellipse, an increase in the longitudinal force of the tire results in a decrease in the lateral force on the tire. As shown in Figure 10g,h,j, at 2 s, the reduction in the lateral force on the tire provides a reverse moment to the vehicle, helping it to return to the right. Finally, the yaw moment provided by the longitudinal force and the lateral force on the tires assists the vehicle to complete the requisite steering operation.

In summary, the simulation results demonstrate that compared to MTTE, the proposed approach can constrain wheel slip and maintain vehicle stability during steering.

5. Discussion

5.1. The Variations in Motor Parameters

The aforementioned results are obtained on the premise that the motor is in an ideal state. In the actual process, as the motor temperature rises and ages, the flux linkage of the motor will decrease, thereby affecting the accuracy of methods that directly control the torque, such as MTTE. As illustrated in Figure 6, T^* is constrained by MTTE to obtain the command torque T_c, and the motor outputs torque T_i based on T_c to drive the vehicle. In this process, T_i will be less than T_c due to the drop in motor flux linkage, which causes the decrease of control accuracy and the loss of vehicle power performance. As for the method proposed here, it controls the motor power tracking command power value inside the motor. It indirectly controls the output torque T_i of the motor so that T_i is in the internal cycle of power following, thus eliminating the effect of variation in the motor magnetic chain.

Figure 11 depicts the variations of vehicle speed and wheel speed for a 10% and 20% drop in flux linkage of the motor for MTTE and the proposed control method under straight line conditions. As demonstrated in Figure 11a, the vehicle speed and wheel speed of the vehicle controlled by MTTE decreased with the drop of the motor flux linkage. When the flux linkage decreases by 10%, the vehicle speed is 19.3 m/s at 5 s; however, when the flux linkage decreases by 20%, the vehicle speed only reaches 18.3 m/s at 5 s. Figure 11b, on the other hand, indicates that the change in motor flux linkage has no effect on the speed of the vehicle when using the proposed control method.

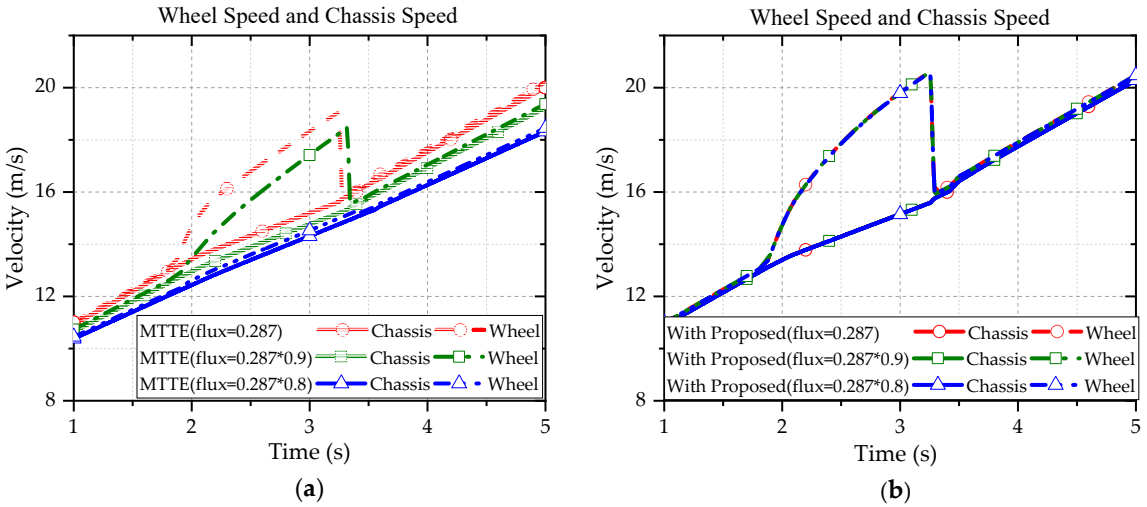

Figure 11. Comparison of wheel speed and chassis speed under the change of flux linkage: (**a**) vehicle with MTTE; (**b**) vehicle with proposed control strategy.

When the vehicle is turning, the reduction in driving torque caused by the change in flux linkage may make an already out-of-control vehicle easier to steer; however, this is not the purpose and result of the anti-skid control method, and it is impossible to predict what effect it will have on the already-controlled vehicle. Therefore, this research only studied whether the change of flux linkage affects the control results and did not explore whether the resulting effect is beneficial. Figure 12 presents the variation in the yaw rate of the vehicle under sine with dwell operating conditions for both control methods with the change of magnetic chain. Figure 12 indicates that the yaw rate of the vehicle with the proposed control method is almost unchanged, while the yaw rate of the vehicle with MTTE control changes significantly.

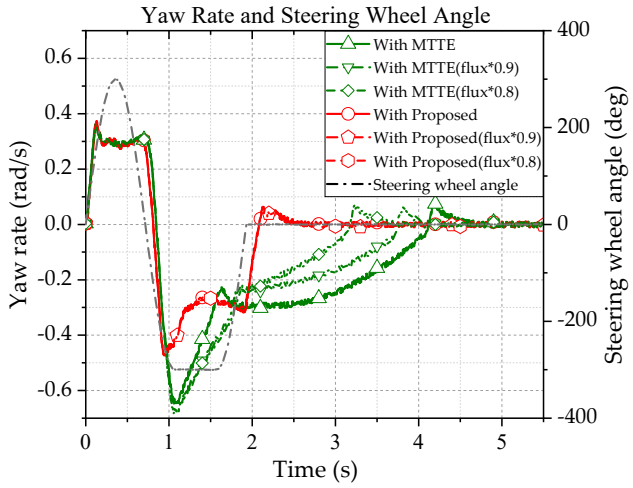

Figure 12. Comparison of the yaw rate between the vehicle with MTTE and with proposed control strategy under the change of flux linkage.

In summary, the control scheme proposed herein, which incorporates motor power following, can counter the effects of changes in the flux linkage of the motor and ensure the accuracy of control, making the method more practical and applicable.

5.2. Vehicle Starting from Standstill

When the vehicle is started from standstill, the vehicle system is in a zero-power condition. In the zero-power condition, if no corresponding measures are taken, the motor will receive a commanded power signal of 0 and cannot output torque. Finally, the vehicle cannot be started. To prevent this from happening, this study adopts a measure by putting restrictions on ω_i^* according to Equations (16) and (17). By doing so, some torque can be delivered to vehicle at zero speed.

$$\omega_i^* = \begin{cases} 5 \cdot sgn(\omega_i), |\omega_i| \le 5 \\ \omega_i, \quad |\omega_i| > 5 \end{cases}, \tag{16}$$

$$sgn(\omega_i) = \begin{cases} -1, \ \omega_i < 0 \\ 1, \ \omega_i \ge 0 \end{cases}. \tag{17}$$

To verify the effectiveness of the above-mentioned method, this study conducts a straight-line driving condition on a road with a friction coefficient of 0.2. The initial speed is set to 0 km/h and the torque command value for a single drive motor is set to 250 N·m. Figure 13 demonstrates that the vehicle can be started properly from standstill with the proposed approach. Simultaneously, the proposed algorithm can quickly detect and suppress wheel slip after the vehicle is started. As shown in Figure 9b, the wheel slip ratio stays near the optimal slip ratio after 1 s, which indicates the algorithm can also maintain the dynamics of the vehicle.

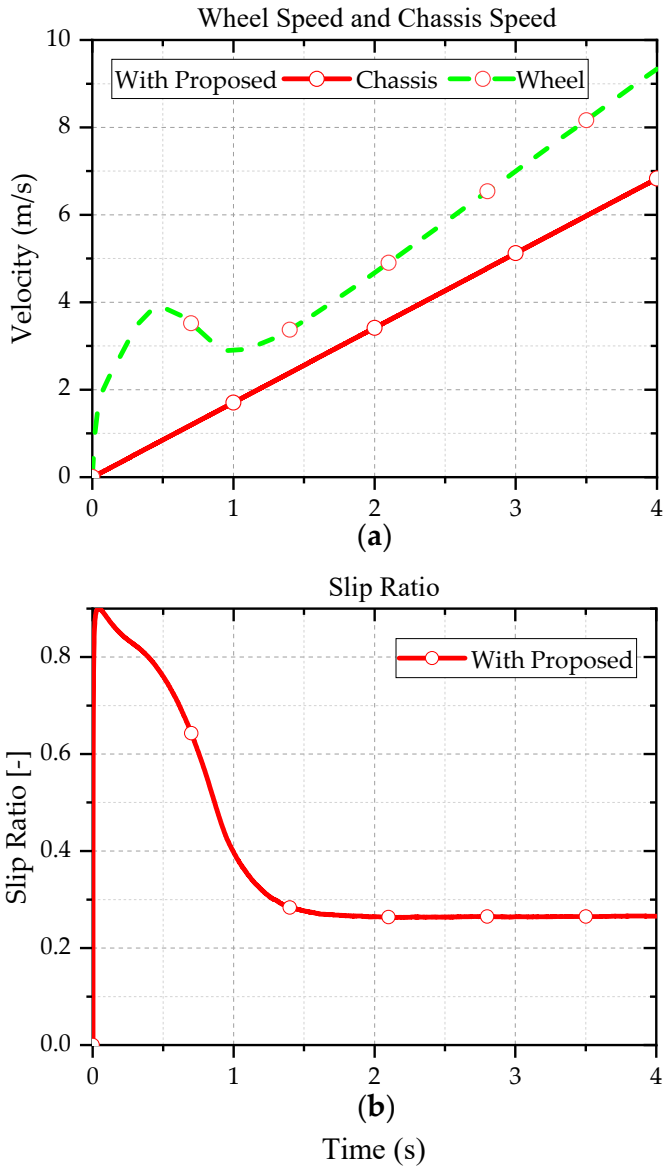

Figure 13. Simulation results of vehicle starting from standstill: (**a**) front-left wheel speed and chassis speed; (**b**) slip ratio of front-left wheel.

6. Conclusions

To improve the anti-slip performance of vehicles in flat motion, the structural characteristics of hub motors and wheels are utilized and a new wheel slip control strategy is proposed for powering decentralized EVs based on the energy method. This method uses the actual and theoretical rotational power consumed by the wheels during motion to regulate output torque.

Simulation results imply that the proposed approach can not only prevent the vehicle from slipping out of control, but also ensure the vehicle's dynamics and steering sensitivity. The comparative simulation further demonstrates that this approach can resist the variability of motor flux linkage, which proves the control stability of this method.

This approach has considerable value for distributed-drive EVs and can improve anti-slip performance and vehicle stability when steering. In the future, further research will be conducted on steering on lower adhesion surfaces, considering more slippery/icy conditions where tire-road friction becomes even more critical. Additionally, the proposed strategy based on energy can also be used to reduce vehicle energy consumption, which will also be studied in future research.

Author Contributions: Conceptualization, D.Y. and L.C.; methodology, D.Y. and L.C.; software, L.C. and Y.Z.; validation, L.C. and Y.Z.; formal analysis, L.C.; investigation, L.C.; resources, L.C. and Y.Z.; data curation, L.C.; writing—original draft preparation, L.C.; writing—review and editing, D.Y. and Y.Z.; visualization, L.C.; supervision, D.Y.; project administration, D.Y.; funding acquisition, D.Y. All authors have read and agreed to the published version of the manuscript.

Funding: This research was funded by "Natural Science Foundation of Jiangsu Province", grant number BK20201307.

Data Availability Statement: Not applicable.

Conflicts of Interest: The authors declare no conflict of interest.

References

1. Ma, S.-C.; Xu, J.-H.; Fan, Y. Characteristics and Key Trends of Global Electric Vehicle Technology Development: A Multi-Method Patent Analysis. *J. Clean. Prod.* **2022**, *338*, 130502. [CrossRef]
2. Bayezit, İ.; Fidan, B. Distributed Cohesive Motion Control of Flight Vehicle Formations. *IEEE Trans. Ind. Electron.* **2013**, *60*, 5763–5772. [CrossRef]
3. Zhuang, W.; Li (Eben), S.; Zhang, X.; Kum, D.; Song, Z.; Yin, G.; Ju, F. A Survey of Powertrain Configuration Studies on Hybrid Electric Vehicles. *Appl. Energy* **2020**, *262*, 114553. [CrossRef]
4. Zhang, X.; Göhlich, D. Integrated Traction Control Strategy for Distributed Drive Electric Vehicles with Improvement of Economy and Longitudinal Driving Stability. *Energies* **2017**, *10*, 126. [CrossRef]
5. Shi, K.; Yuan, X.; Liu, L. Model Predictive Controller-Based Multi-Model Control System for Longitudinal Stability of Distributed Drive Electric Vehicle. *ISA Trans.* **2018**, *72*, 44–55. [CrossRef]
6. Liu, J.; Zhong, H.; Wang, L.; Chen, H. *A Novel Torque Distribution Strategy for Distributed-Drive Electric Vehicle Considering Energy Saving and Brake Stability*; SAE Technical Paper: Warrendale, PA, USA, 2019.
7. Yin, D.; Sun, N.; Hu, J.-S. A Wheel Slip Control Approach Integrated with Electronic Stability Control for Decentralized Drive Electric Vehicles. *IEEE Trans. Ind. Inform.* **2019**, *15*, 2244–2252. [CrossRef]
8. Zhang, D.; Song, Q.; Wang, G.; Liu, C. A Novel Longitudinal Speed Estimator for Four-Wheel Slip in Snowy Conditions. *Appl. Sci.* **2021**, *11*, 2809. [CrossRef]
9. Li, J.; Wang, C.; Zhang, J. Wheel Slip Tracking Control of Vehicle Based on Fast Terminal Sliding Mode State Observer. *J. Hunan Univ. Nat. Sci.* **2020**, *47*, 14–23.
10. Rajendran, S.; Spurgeon, S.K.; Tsampardoukas, G.; Hampson, R. Estimation of Road Frictional Force and Wheel Slip for Effective Antilock Braking System (ABS) Control. *Int. J. Robust Nonlinear Control* **2019**, *29*, 736–765. [CrossRef]
11. Pichlík, P.; Bauer, J. Adhesion Characteristic Slope Estimation for Wheel Slip Control Purpose Based on UKF. *IEEE Trans. Veh. Technol.* **2021**, *70*, 4303–4311. [CrossRef]
12. Hu, J.; Liu, Y.; Xiao, F.; Lin, Z.; Deng, C. Coordinated Control of Active Suspension and DYC for Four-Wheel Independent Drive Electric Vehicles Based on Stability. *Appl. Sci.* **2022**, *12*, 11768. [CrossRef]
13. Yeong, D.J.; Velasco-Hernandez, G.; Barry, J.; Walsh, J. Sensor and Sensor Fusion Technology in Autonomous Vehicles: A Review. *Sensors* **2021**, *21*, 2140. [CrossRef]
14. Ding, X.; Zhang, L.; Wang, Z.; Liu, P. Acceleration Slip Regulation for Four-Wheel-Independently-Actuated Electric Vehicles Based on Road Identification through the Fuzzy Logic. *IFAC-Pap.* **2018**, *51*, 943–948. [CrossRef]
15. Fujii, K.; Fujimoto, H. Traction Control Based on Slip Ratio Estimation without Detecting Vehicle Speed for Electric Vehicle. In Proceedings of the 2007 Power Conversion Conference—Nagoya, Nagoya, Japan, 2–5 April 2007; pp. 688–693.
16. Xu, G.; Xu, K.; Zheng, C.; Zahid, T. Optimal Operation Point Detection Based on Force Transmitting Behavior for Wheel Slip Prevention of Electric Vehicles. *IEEE Trans. Intell. Transp. Syst.* **2016**, *17*, 481–490. [CrossRef]
17. Pomoni, M. Exploring Smart Tires as a Tool to Assist Safe Driving and Monitor Tire—Road Friction. *Vehicles* **2022**, *4*, 744–765. [CrossRef]
18. Sakai, S.-I.; Hori, Y. Advantage of Electric Motor for Anti Skid Control of Electric Vehicle. *EPE J.* **2001**, *11*, 26–32. [CrossRef]
19. Fujimoto, H.; Saito, T.; Noguchi, T. Motion Stabilization Control of Electric Vehicle under Snowy Conditions Based on Yaw-Moment Observer. In Proceedings of the 8th IEEE International Workshop on Advanced Motion Control, 2004. AMC '04, Kawasaki, Japan, 28 March 2004; pp. 35–40.
20. Yin, D.; Sun, N.; Shan, D.; Hu, J.-S. A Multiple Data Fusion Approach to Wheel Slip Control for Decentralized Electric Vehicles. *Energies* **2017**, *10*, 461. [CrossRef]
21. Yin, D.; Oh, S.; Hori, Y. A Novel Traction Control for EV Based on Maximum Transmissible Torque Estimation. *IEEE Trans. Ind. Electron.* **2009**, *56*, 2086–2094. [CrossRef]
22. Li, J.; Song, Z.; Shuai, Z.; Xu, L.; Ouyang, M. Wheel Slip Control Using Sliding-Mode Technique and Maximum Transmissible Torque Estimation. *J. Dyn. Syst. Meas. Control* **2015**, *137*, 111010. [CrossRef]
23. Hu, J.-S.; Yin, D.; Hori, Y. Electric Vehicle Traction Control—A New MTTE Approach with PI Observer. *IFAC Proc. Vol.* **2009**, *42*, 137–142. [CrossRef]

24. Jiang, B.; Sharma, N.; Liu, Y.; Li, C. Acceleration-Based Wheel Slip Control Realized with Decentralised Electric Drivetrain Systems. *IET Electr. Syst. Transp.* **2022**, *12*, 143–152. [CrossRef]
25. Awan, H.A.A.; Saarakkala, S.E.; Hinkkanen, M. Flux-Linkage-Based Current Control of Saturated Synchronous Motors. *IEEE Trans. Ind. Appl.* **2019**, *55*, 4762–4769. [CrossRef]
26. Zhi, J. Research on Skid Steering and Driving Control for the Multi-wheel-drive Vehicle. Ph.D. Thesis, Beijing Institute of Technology, Beijing, China, 2016.
27. Picot, N.; Miller, B.; Rizzo, M.D.; Klingler, T.A. FMVSS126 Electronic Stability Control Sine with Dwell Incomplete Vehicle Type 2 Analysis. *SAE Int. J. Passeng. Cars—Mech. Syst.* **2011**, *4*, 713–721. [CrossRef]